Supporting Information

Carbon Nitride-based Light-driven Microswimmers with Intrinsic Photocharging Ability

Varun Sridhar[1 †], Filip Podjaski[2 †], Julia Kröger[2,3], Alberto Jiménez-Solano[2], Byung-Wook Park[4], Bettina V. Lotsch[2,3]*, and Metin Sitti[1,5,6]*

[1] Physical Intelligence Department, Max Planck Institute for Intelligent Systems, 70569 Stuttgart, Germany
[2] Nanochemistry Department, Max Planck Institute for Solid State Research, 70569 Stuttgart, Germany
[3] Department of Chemistry, University of Munich (LMU), Munich, Germany
[4] Department of Chemical Engineering, Youngstown State University, Ohio, USA
[5] School of Medicine and School of Engineering, Koç University, 34450 Istanbul, Turkey
[6] Institute for Biomedical Engineering, ETH Zurich, 8092 Zurich, Switzerland

[†] Equally contributing first authors

*Correspondence to: sitti@is.mpg.de, b.lotsch@fkf.mpg.de

Keywords: Carbon nitrides, light-driven, microswimmers, photocharging, solar battery, organic semiconductors

www.pnas.org/cgi/doi/10.1073/pnas.2007362117

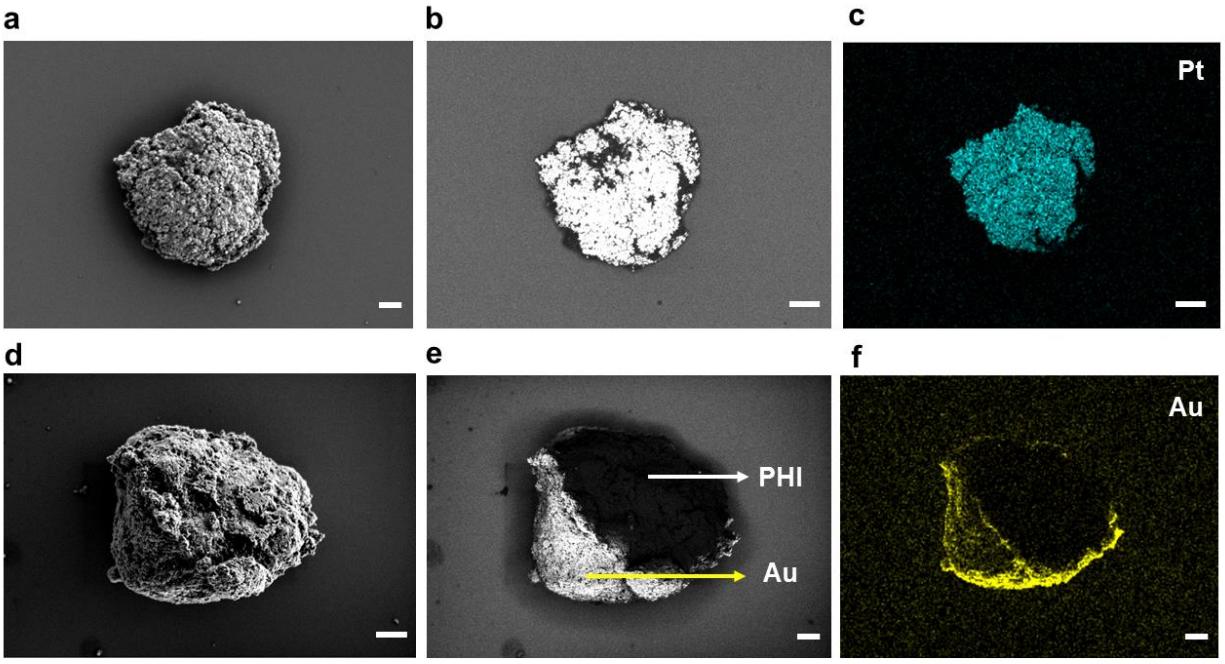

Figure S1. SEM and EDX images of Janus PHI microswimmers. **a)** Secondary electron image of a PHI-Pt Janus particle lying with the Pt face up and **b)** its corresponding back-scattered electron image highlighting the distribution of Pt by bright contrast. **c)** EDX map of a PHI-Pt Janus particle highlighting the presence of Pt on the Janus microswimmer in blue. **d)** Secondary electron image of PHI-Au Janus particle lying on its side. **e)** Corresponding back-scattered electron image highlighting the distribution of Au by bright contrast and **f)** EDX map of a PHI-Au Janus particle highlighting the presence of Au on the Janus microswimmer in yellow. The EDX detector is placed on the side of the chamber, thus causing shading effects. Scale bar: 1 µm.

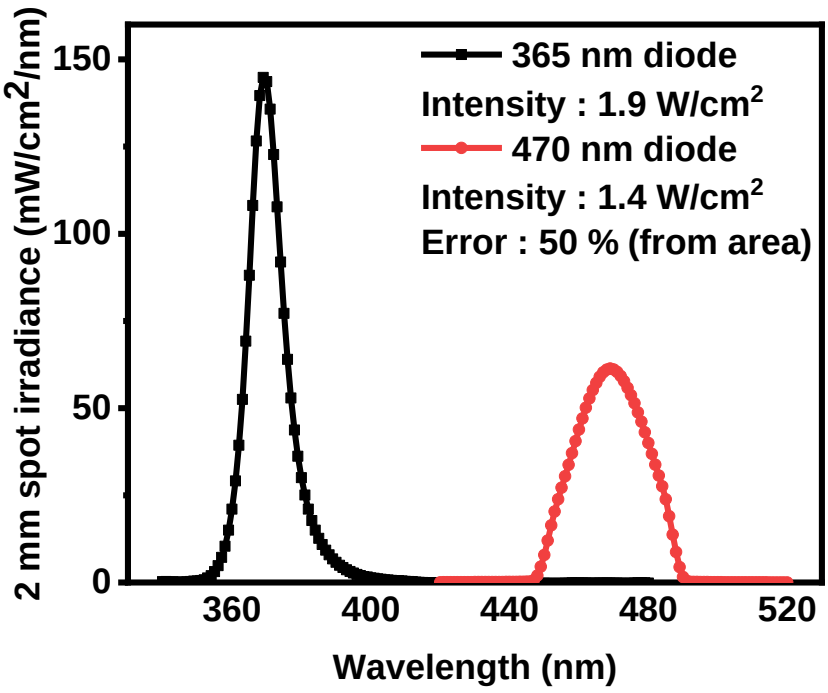

Figure S2: Spectral irradiance and resulting intensity of the light sources used for propulsion of the microswimmers, measured at the place of the sample (see Materials and Methods for more information).

Supplementary Note 1: Magnetic steering control

Directional control (steering) of light-driven microswimmers is important for environmental and biomedical applications, where the phototaxis of the microswimmers is difficult to control under *in-vivo* conditions. There are two major methods of controlling the motion direction of microswimmers: phototaxis using light and magnetic control (magnetotaxis) using an external magnetic field. In the case of self-electrophoretic microswimmers, magnetic control makes the directional motion easy and possible. For the PHI microswimmers, it can be achieved by adding a ferromagnetic Ni layer between the PHI and the Pt cap layers. For this purpose, a 5 nm-thin layer Ni is sputtered on the PHI nanoparticle before the Pt layer. When PHI-Ni-Pt microswimmers are exposed to a small, uniform external magnetic field (~8 mT), they start to follow the direction of the applied magnetic field, as shown in the snapshots in Figure **S3** and Supplementary Movie **1**. The porous and imperfect spherical nature of the microswimmer may cause tumbling motion when the magnetic field is applied. Hence, they do not always immediately follow the direction of the applied magnetic field.

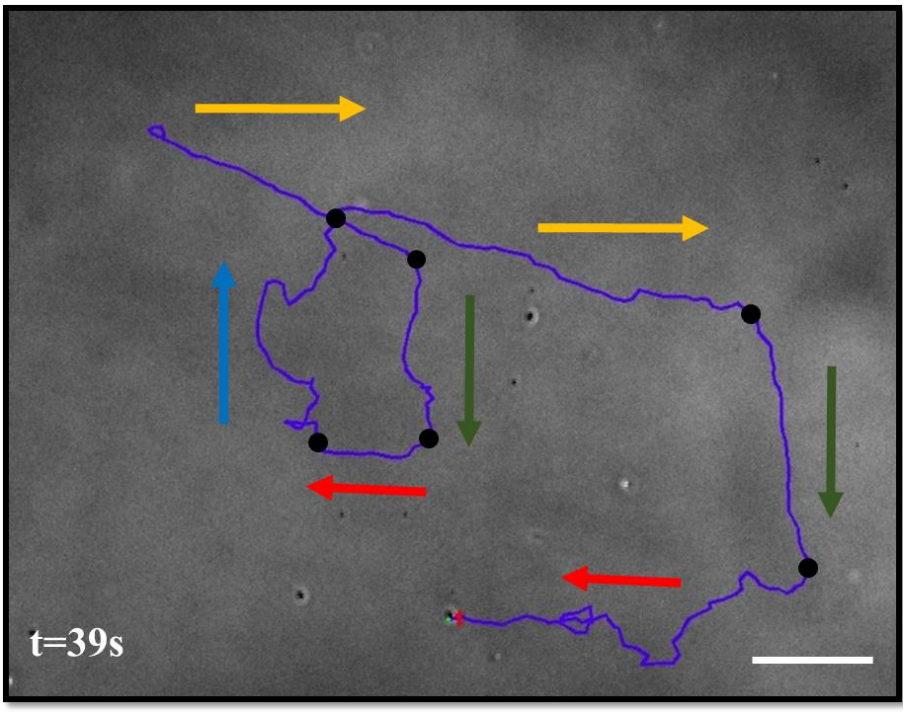

Figure S3: Video snapshots of the magnetically guided PHI-Ni-Pt microswimmer (from Supporting Movie 1) under the UV light at various time intervals with 5% methanol (MeOH), with the black dots indicating the time points where the uniform 8 mT magnetic field changes direction (indicated by colored arrows). Scale bar: 5 μm.

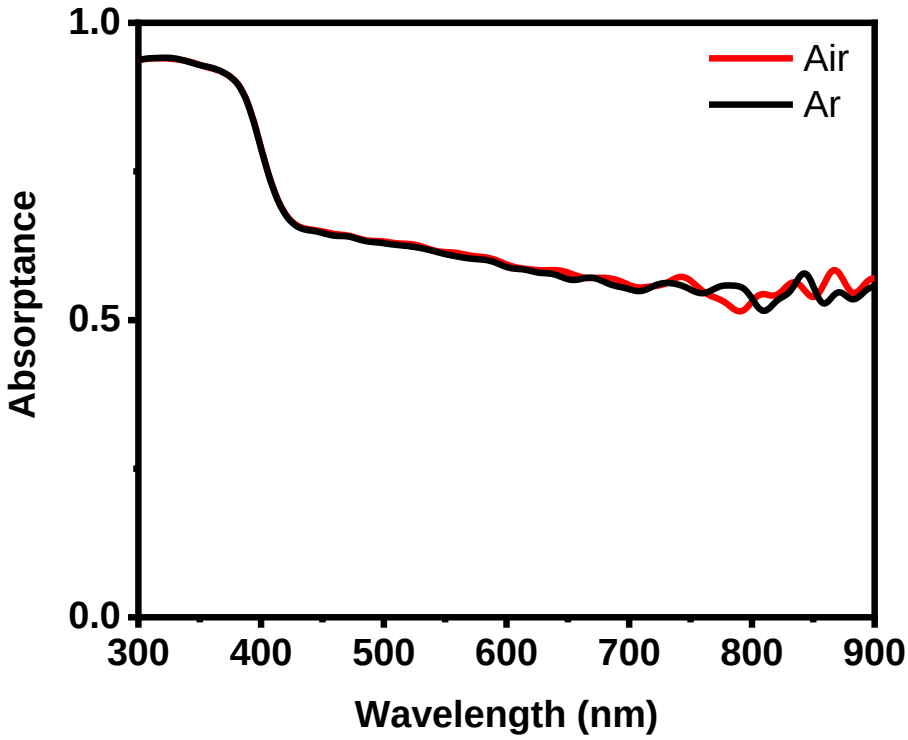

Figure S4: Absorptance of a PHI-Pt microswimmer suspension in water with and without O_2. The absorption onset of PHI is ~450 nm.

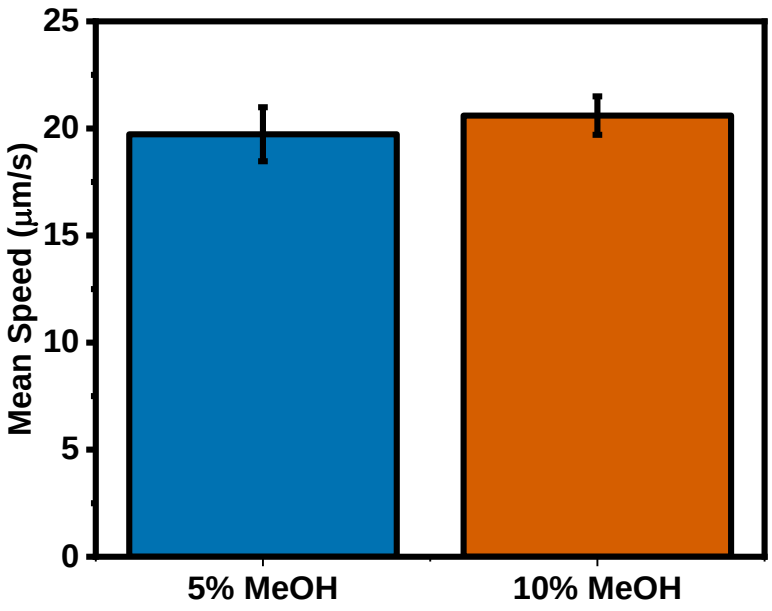

Figure S5: Average mean speed of PHI-Pt microswimmers under UV illumination with different MeOH concentrations.

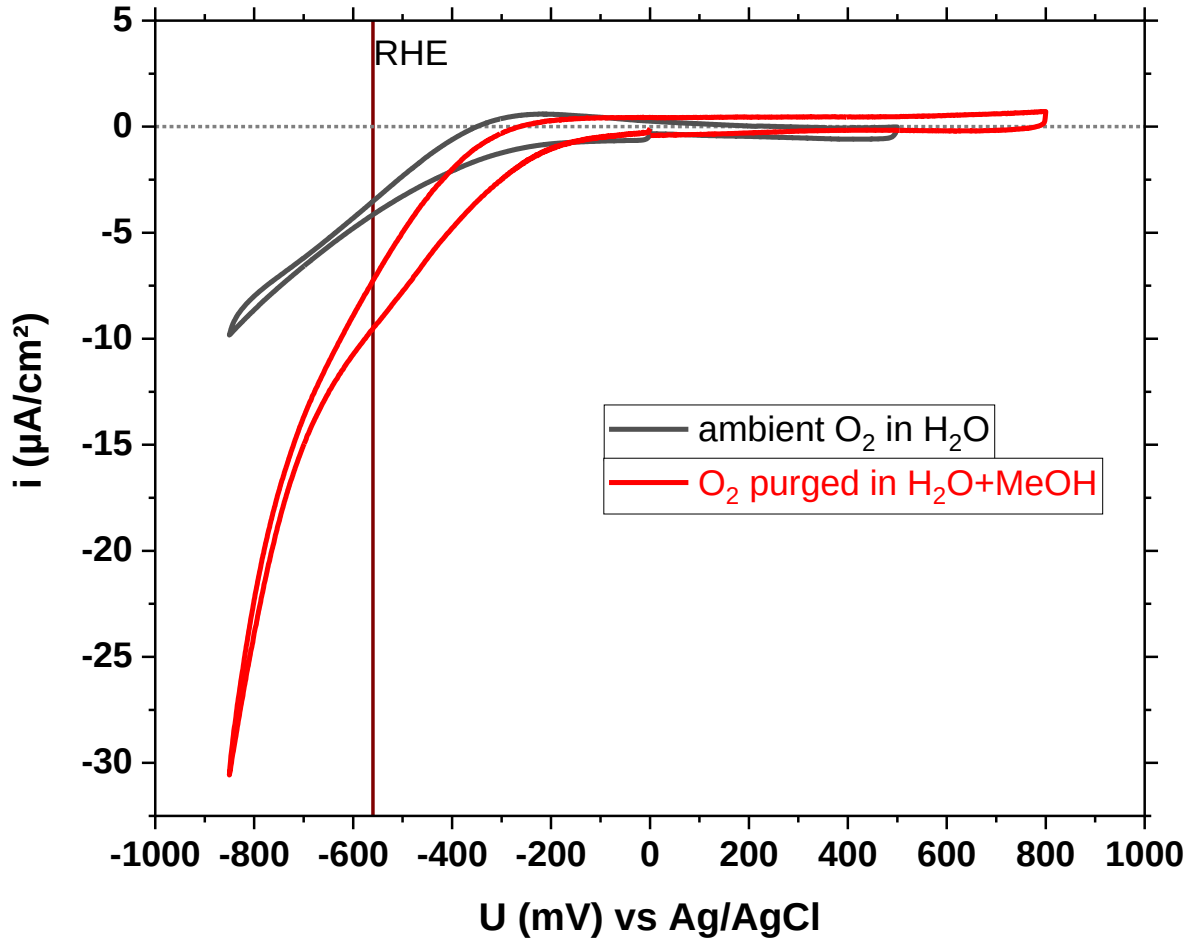

Figure S6: Electrochemical cyclic voltammogram (CV) of PHI deposited on fluorine-doped tin oxide glass (FTO) in deionized water. Purging with oxygen further increases the reductive currents, which start at approx. -200mV vs Ag/AgCl, i.e. well before the RHE. MeOH does not affect the currents in this potential window. The dark currents originating from FTO alone in O_2 containing conditions are of comparable magnitude to these with PHI deposited on FTO, which is attributed to comparably slow charge transfer kinetics of the PHI when reacting with oxygen.

Supplementary Note 2: Oxygen reduction reaction (ORR)

Upon photoexcitation, many semiconductors such as TiO_2 and CN_x can reduce dissolved oxygen on their own or on a Pt surface, by driving the oxygen reduction reaction (ORR) or by producing reactive oxygen species (ROS), which then react further and are often used for the removal of pollutants.(1, 2) This thermodynamically downhill reaction is in competition with solar fuel productions since the scavenging of electrons by O_2 impedes uphill photosynthetic reactions, such as the hydrogen evolution reaction or the CO_2 reduction.(3)·(4)

The ORR has thermodynamically the highest driving force, but it requires the transfer of four electrons:

E^0 (O_2/H_2O) = +1.23 V vs SHE @ 1 bar O_2 (Nernstian pH dependence)

The main ROS formed upon reduction of O_2 are (1) superoxide radicals ($^{\bullet}O_2^-$), which are in equilibrium with (2) hydroperoxyl radicals ($^{\bullet}HO_2$) in acidic conditions ($^{\bullet}HO_2$ <-> $^{\bullet}O_2^-$ + H^+), as well as (3) hydroxyl radicals ($^{\bullet}HO$), which are formed by the decomposition of hydrogen peroxide (H_2O_2 <-> 2 $^{\bullet}HO$). Hydrogen peroxide itself can be a product of the ROS formation and further reduction, as listed in the reduction reaction potentials below. The equilibrium potentials of the main ROS are:(5),(2)

E^0 ($O_2/^{\bullet}O_2^-$) = -0.33 V vs SHE @ 1 bar O_2 (constant if pH > 4.8)
E^0 ($O_2/^{\bullet}O_2^-$) = -0.16 V vs SHE @ 1 M O_2

E^0 ($O_2/^{\bullet}HO_2$) = -0.037 V vs SHE @ pH 0

These ROSs can then further react to form other radicals or hydrogen peroxide(2),(1)

E^0 ($^{\bullet}O_2^-/H_2O_2$) = +0.94 V vs SHE @ pH 7
E^0 ($^{\bullet}O_2^-/HO_2^-$) = +1 V vs SHE

E^0 ($^{\bullet}HO_2/H_2O_2$) = +1.42 V vs SHE @ pH 0; +1 V vs SHE @ pH 7
E^0 ($^{\bullet}HO_2/HO_2^-$) = +0.79 V vs SHE

Subsequent reactions with H_2O_2 are discussed in Supplementary Note **5**. The hydroxyl radical, which is in equilibrium with H_2O_2 (H_2O_2 <-> 2 $^{\bullet}HO$), can also be reduced further:

E^0 ($^{\bullet}OH/OH^-$) = +1.9 V vs SHE

Besides, also the formation of the ROS singlet oxygen ($^1O_2$) via H_2O_2 is possible via photosensitization.(6)

A more detailed overview of the energetics of reductive processes involving O_2 at pH 7 is reported elsewhere.(7)

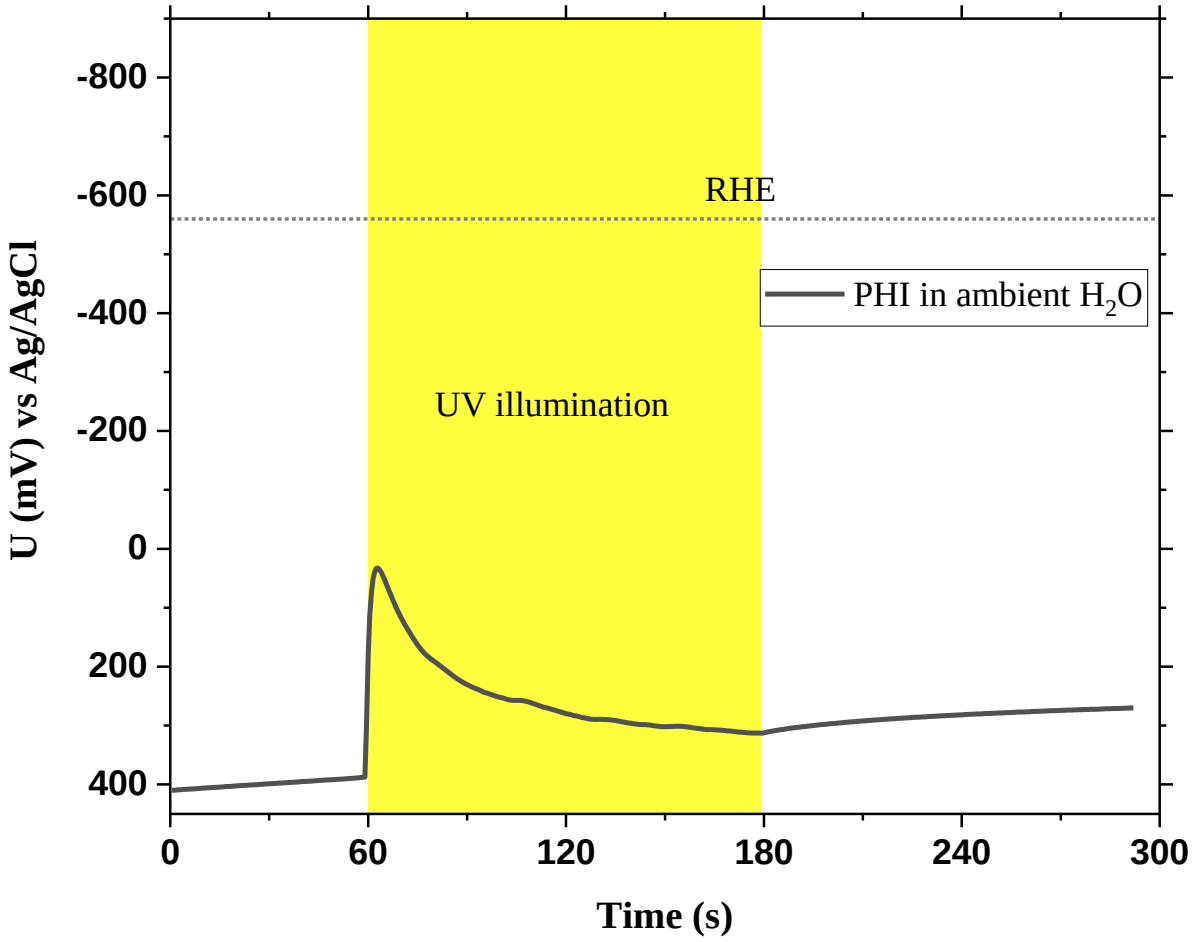

Figure S7: Transient open circuit potential (OCP) measurement of a thick layer of PHI deposited on FTO in DI water. Upon illumination, an OCP shift is generated by illumination. Subsequently, electrons react with oxygen, lowering the OCP under illumination.

Supplementary Note 3: Light-induced propulsion without added alcohol

To further investigate the propulsion without alcohol present, open circuit potential (OCP) measurements of a PHI film deposited on fluorine-doped tin oxide glass (FTO) were performed in water under ambient conditions (Figure **S7**). After a fast negative spike upon illumination towards 0 V vs Ag/AgCl due to photogeneration of charge carriers, a continuous positive shift down to +300 mV vs Ag/AgCl is observed, evidencing the extraction of electrons by oxygen, balancing the hole reaction entirely.

In order to evidence the water oxidation reaction (OER) enabling donor free propulsion with metal caps, cyclic voltammograms (CVs) were performed under chopped illumination under more oxidative potentials (Figure **S8**). An oxidative photocurrent could be measured at potentials more positive than +1V vs. Ag/AgCl, since only then, a high enough driving force for electron extraction

is provided, avoiding excessive charge recombination that also impedes the measurement of photocurrents at more negative potentials than +1V.

The fact that enhanced light induced propulsion in pure water was only observed with metal caps and not with SiO_2 can be rationalized by the fact that these metal caps act as electron sinks and hence decrease the charge recombination on the PHI side if the hole reaction is rate limiting. This enables enhanced oxidation reaction rates on the organic semiconductor part, while the metal caps also drive the reduction reaction, leading to self-electrophoretic propulsion with the charge carriers separated at the metal-semiconductor interface.

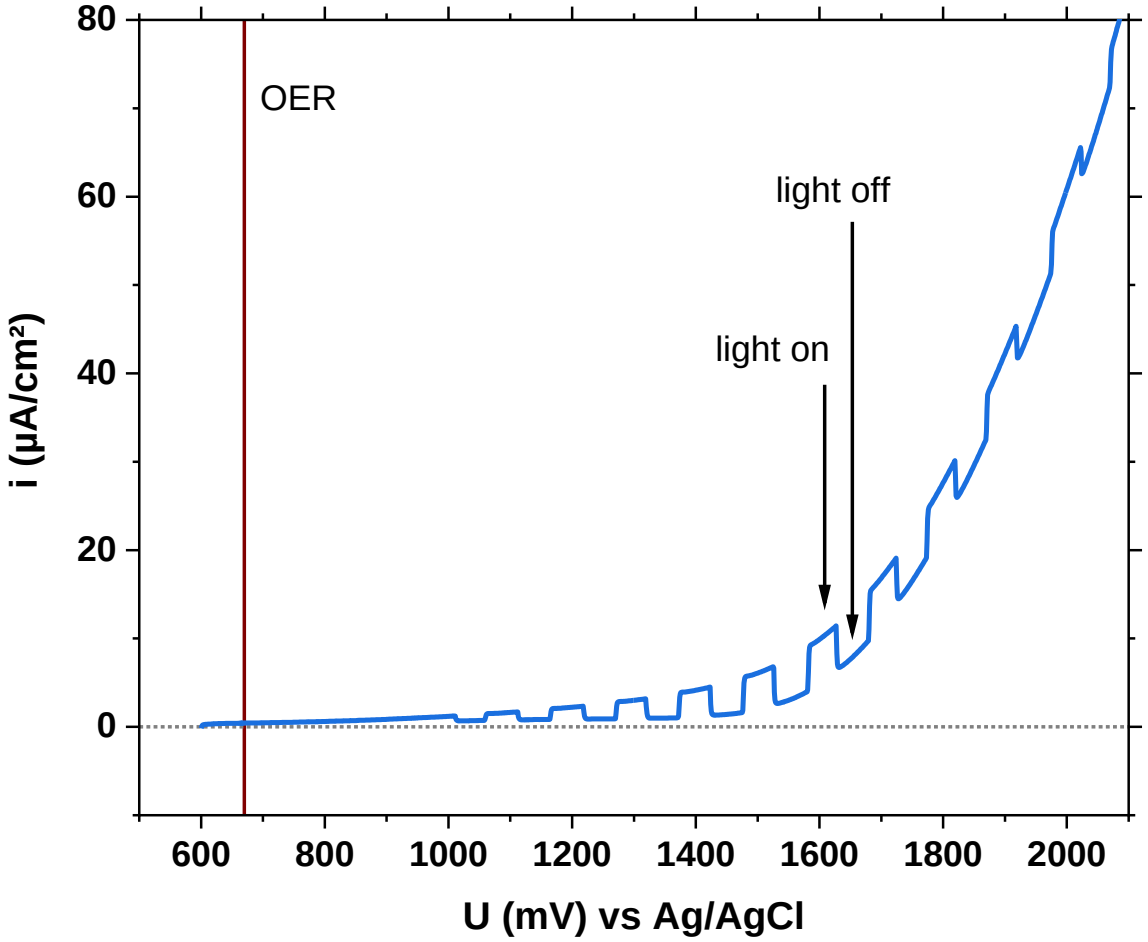

Figure S8: Cyclic voltammogram of PHI deposited on FTO substrate in deionized (DI) water in the oxidation region. As evidenced by the positive photocurrent upon chopped illumination, a water oxidation reaction can take place on the PHI surface after photon absorption. Since the photocurrents are comparably small and the reaction overpotential is rather high, it can be assumed that the water oxidation is rate limiting when no donor is present.

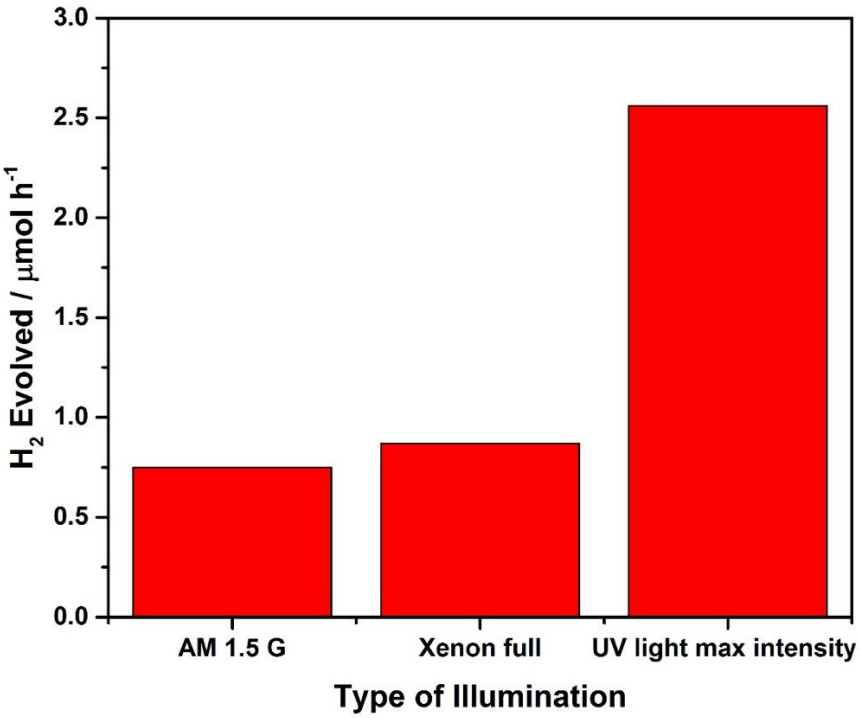

Figure S9: Hydrogen evolution measurements of PHI-Pt microswimmer with 10% MeOH in O_2-free conditions, under AM 1.5 G illumination, with the full spectrum of the same xenon lamp and with UV light (same conditions as for light induced swimming measurements).

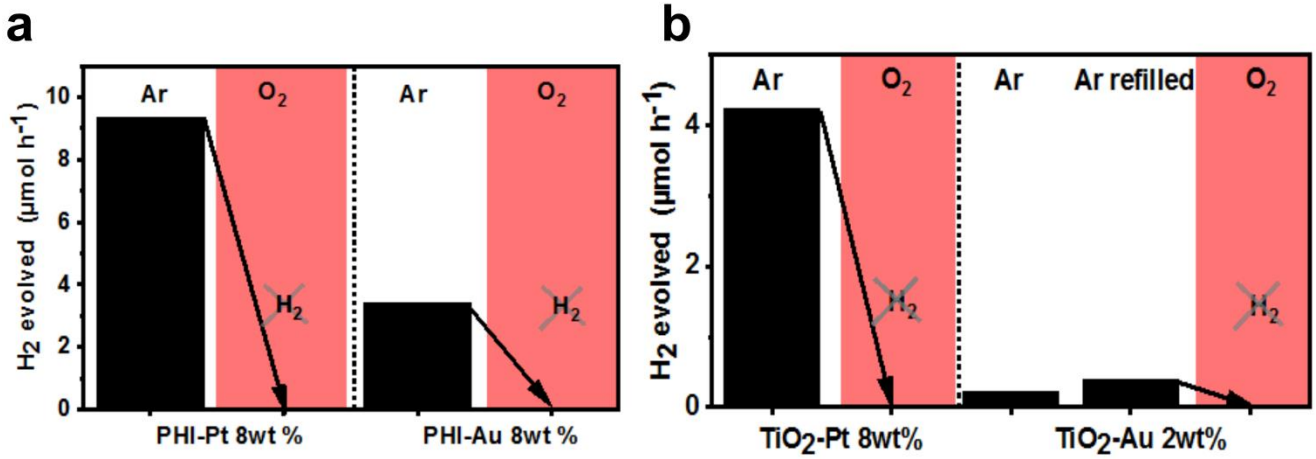

Figure S10: Hydrogen evolution measurements of PHI (**a**) and anatase TiO_2 (**b**) with photo-deposited Pt or Au in water containing 10% MeOH under Xe full arc illumination (100 mW/cm²). Hydrogen evolution is only observed in degassed conditions (Ar). In ambient, oxygen containing conditions (red background), no H_2 was observed.

Supplementary Note 4: Hydrogen evolution reaction

In oxygen free environments, the ORR can be excluded and the dominant surface reaction on the metal caps becomes the hydrogen evolution reaction, as long as only alcohol donors are used to quench photogenerated holes. PHI-Pt microswimmers were tested for hydrogen evolution with 10% MeOH under different illumination intensities and their hydrogen evolution rates are shown in Figure S**7**. In general, more hydrogen was evolved with increasing intensity of UV light. The hydrogen evolution rate increased from 0.75 µmol h^{-1} with an AM1.5 G filter to 0.87 µmol h^{-1} with the full range illumination wavelength of a Xe-lamp. A further drastic increase was observed with the UV lamp (2.56 µmol h^{-1}). Comparing those hydrogen evolution rates to literature, the Janus PHI-Pt microswimmers show a lower photocatalytic activity in comparison to classical photocatalysis experiment with *in-situ* Pt photo-deposition (1200 µmol h^{-1} g^{-1}), although a normalization is difficult since the amount of PHI cannot be determined correctly after Pt cap deposition. A decrease in activity with respect to in-situ Pt deposition might be due to different particle sizes and less accessible surface area of both, CN_x and Pt. Light is scattered or absorbed and thermalized by the sputtered metal cap instead of being absorbed by the PHI (see Figure **S4**). In the presence of ambient oxygen as seen in Figures **2f** and **S10**, no hydrogen evolution was observed further validating the role of ORR in the propulsion of microswimmers.

Supplementary Note 5: Possible redox-reactions with H_2O_2

As stated in Supplementary Note 3, H_2O_2 can be a product of the formation of a ROS, but since the concentration of products formed due to photocatalytic propulsion with microswimmers stays rather very low, this discussion focusses on H_2O_2 being an added fuel in concentrations >0.01 vol%. Besides being used as donor species in order to facilitate hole extraction from semiconductor photocatalysts compared to the OER,(8) it can also be reduced easily, acting as electron acceptor.(9),(3)

The main reduction reactions with conduction band electrons (e^-_{CB}) are:(8)

$H_2O_2 + e^-_{CB} \rightarrow OH^- + OH^\bullet$ (1)

$OH^- + OH^\bullet + e^-_{CB} + 2H^+ \rightarrow 2\ H_2O$ (2)

Whereas the most dominant reactions with valence band holes (h^+_{VB}) are the following:

$H_2O_2 + h^+_{VB} \rightarrow O_2^{\bullet-} + 2H^+$ (3)

$H_2O_2 + 2\ h^+_{VB} \rightarrow 2H^+ + O_2$ (4)

Besides, hydrogen peroxide can react with its own ROS (H_2O_2 <-> 2 $^\bullet$HO):

$H_2O_2 + OH^\bullet \rightarrow {}^\bullet O_2H + H_2O$ (5)

${}^\bullet O_2H + OH^\bullet \rightarrow H_2O + O_2$ (6)

Further information about the reaction mechanisms that can occur on the surface of PHI microswimmers and their metal caps in the presence of H_2O_2 can be found in the literature.(10) (11)

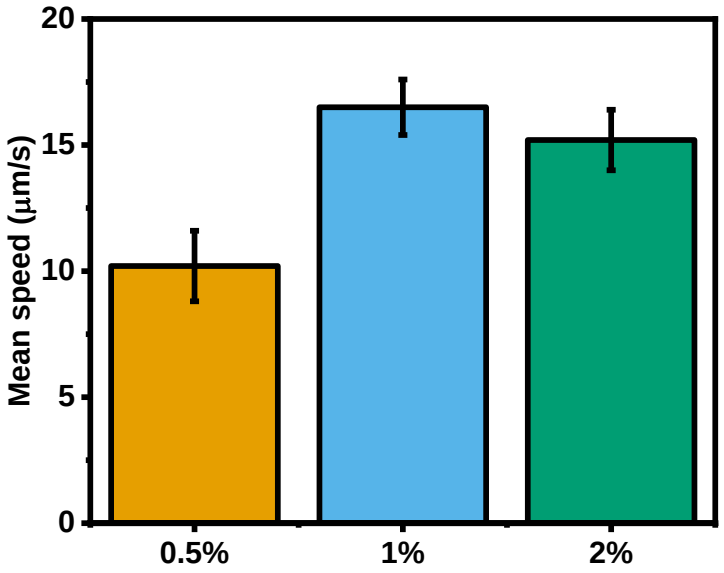

Figure S11: Mean speed of PHI-Pt microswimmers under different H_2O_2 concentrations under UV illumination.

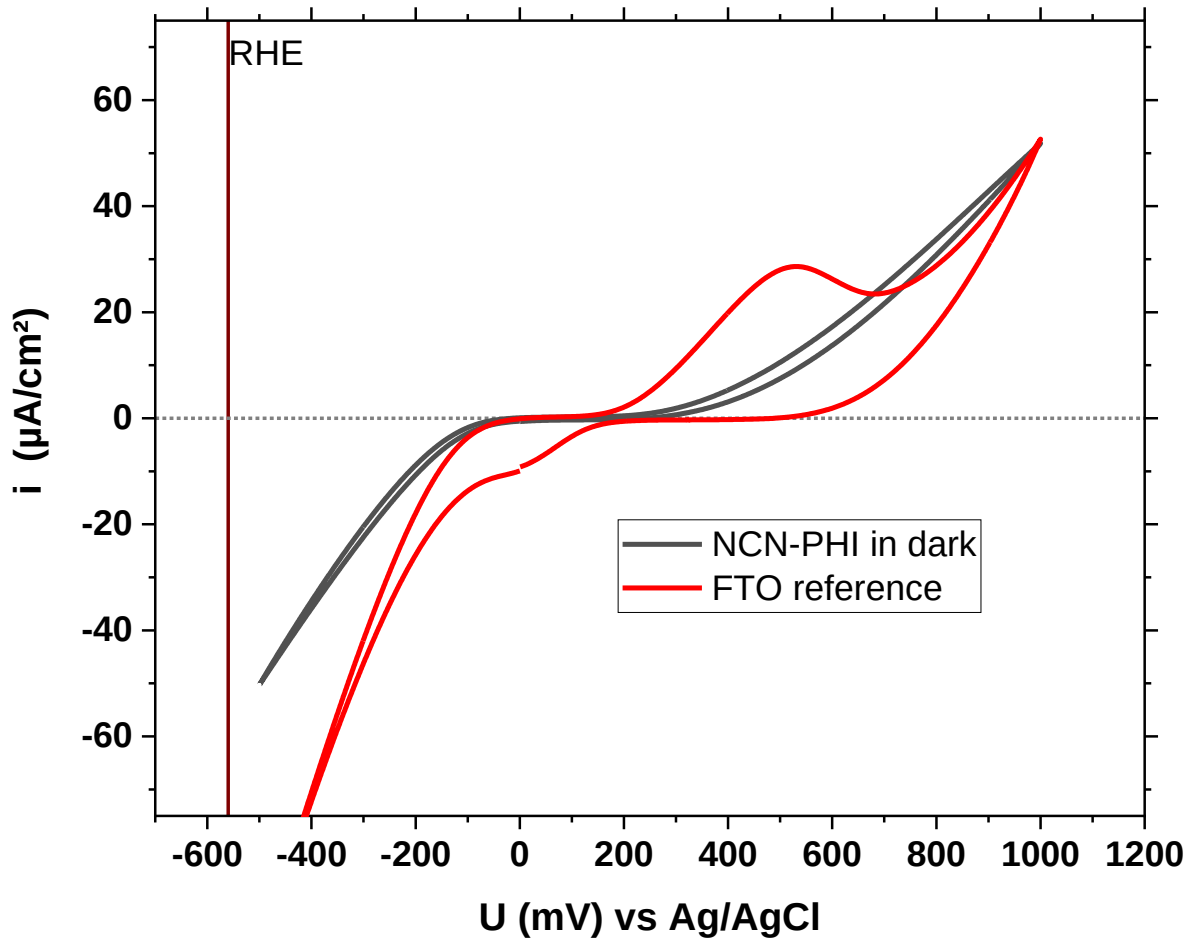

Figure S12: Dark currents of a bare FTO substrate and one covered with PHI nanosheets (10 µg) in DI water containing 1 vol% H_2O_2.

Supplementary Note 6: Photoelectrochemistry of FTO in H_2O_2

From the dark blank experiments (Figure **S12**), it can be seen that the reduction and oxidation of H_2O_2 in the dark occurs in a small voltage window (negative of -100 and positive of +300mV vs Ag/AgCl, respectively). Since H_2O_2 reduction occurs positive of the onset of ORR (-200 mV vs. Ag/AgCl, Figures **2c** and **S6**), oxygen can play only a minor role in the propulsion mechanism in this case and is hence neglected in the following, since it does not affect the faster H_2O_2 reduction severely. (9)

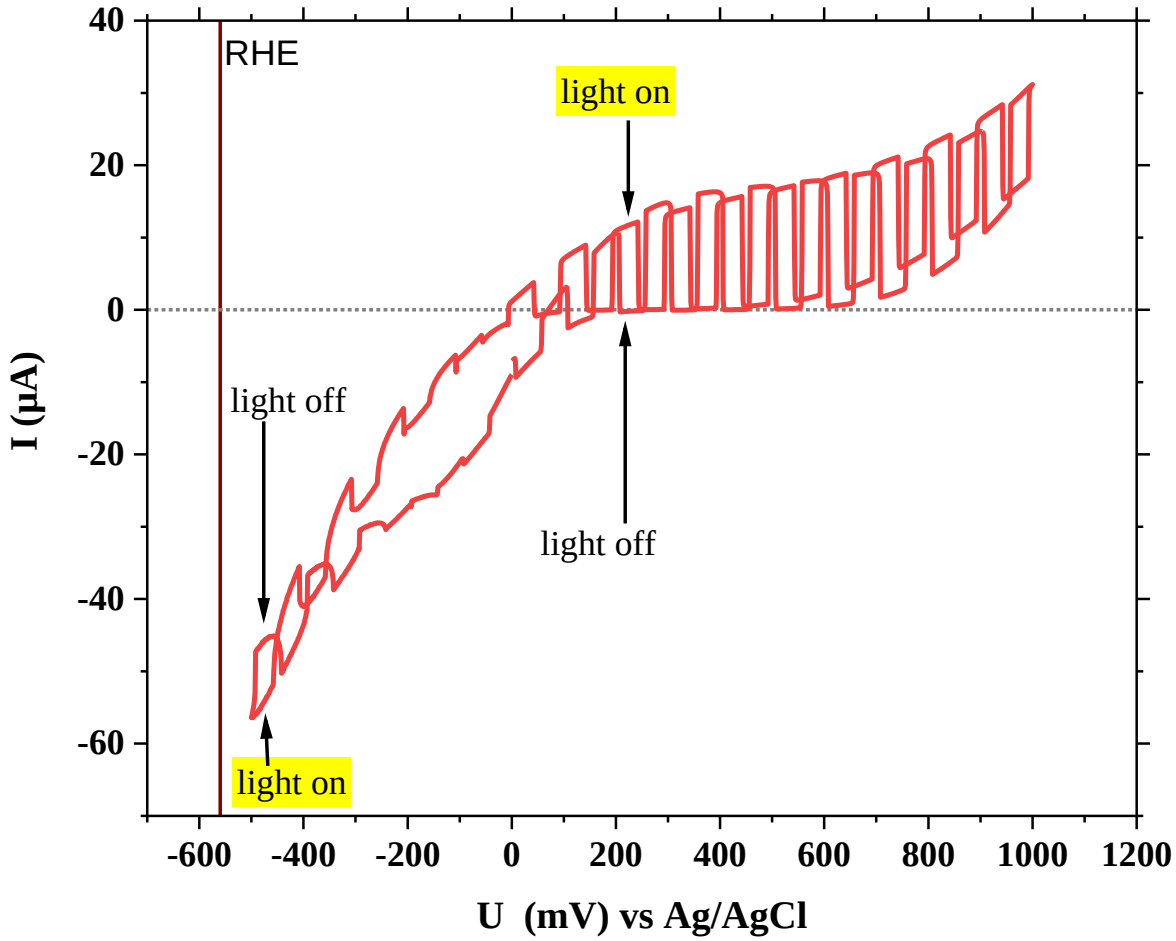

Figure S13: Cyclic voltammogram of PHI nanosheets (10 µg) deposited on FTO substrate in DI water containing 1 vol% H_2O_2 under intermittent UV illumination. A shift from photooxidation to photoreduction is visible at approximately 0 V vs. Ag/AgCl. A stronger oxidative photocurrent suggests this reaction to be more efficient on the surface of PHI. Since the photocurrent actually only shows the imbalance of photogenerated electrons or holes extracted by the potentiostat and both charges can react with H_2O_2, opposite to the case of MeOH without O_2, a photocurrent of similar size implies that the real surface reaction rate is much higher than the photocurrent alone with H_2O_2. Consequently, the light induced surface reaction kinetics are also much faster than the ones mesured with MeOH, since there, the electrons cannot decay by surface reactions.

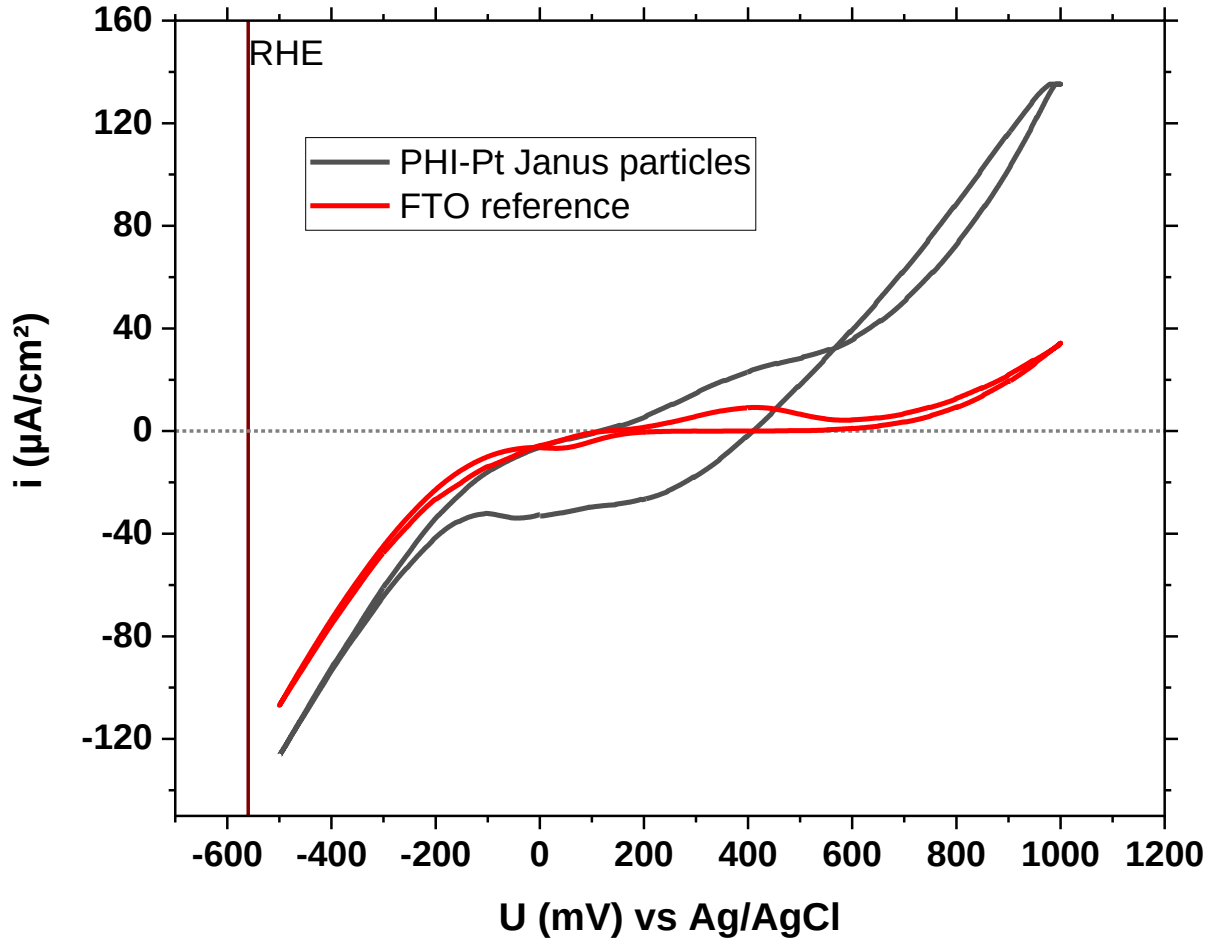

Figure S14: Cyclic voltammogram of PHI-Pt Janus particles deposited on FTO substrate in DI water containing 1 vol% H_2O_2 in comparison to a blank FTO substrate.

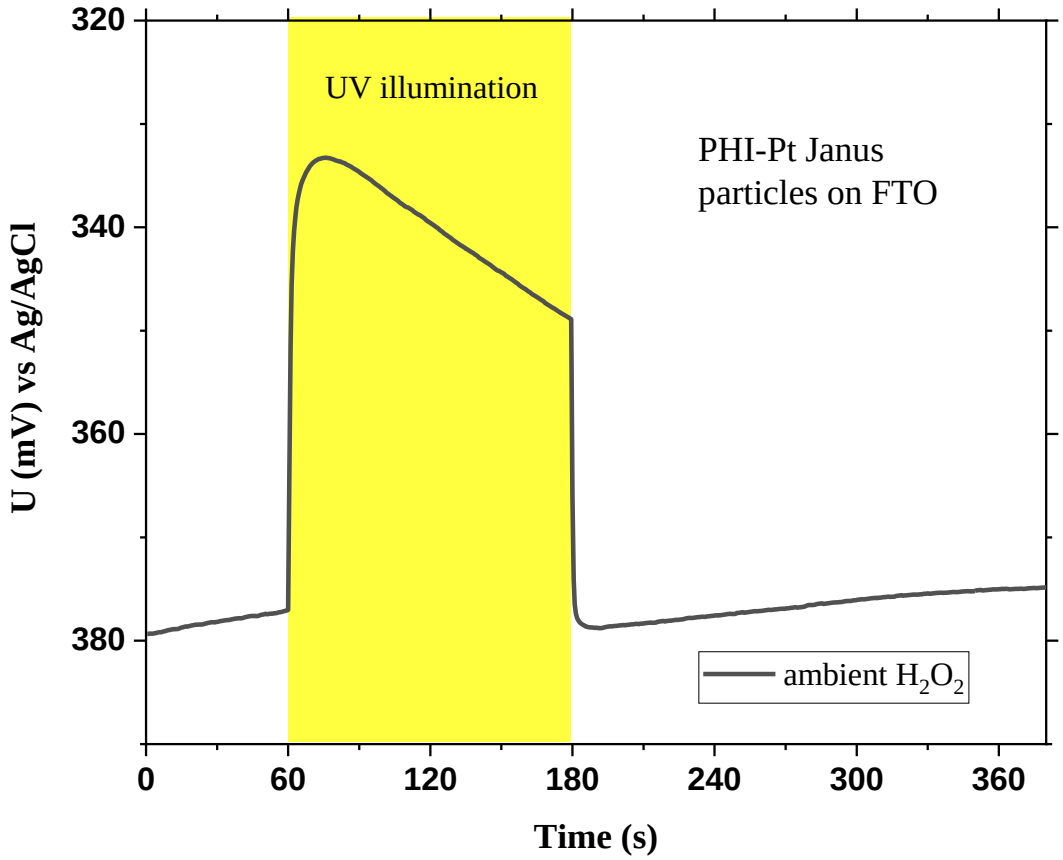

Figure S15: Open circuit potential measurement of PHI-Pt Janus particles deposited on FTO substrate before, during and after UV illumination.

Supplementary Note 7: Photoelectrochemistry with PHI in H_2O_2

In the case of a Pt or Au cap and a bulky Janus particle deposited on FTO, the situation is different from pure PHI sheets on FTO, since the cap material can accept the electrons and holes from PHI and drive the reduction or oxidation of H_2O_2, impeding the analysis of photoelectrochemical responses via the FTO substrate. Furthermore, the noble metal on the Janus particle increases the dark currents significantly, as shown in Figure **S12** for PHI-Pt Janus particles, due to the high redox activity of Pt in contact with H_2O_2. Consequently, also most photogenerated charges react without being measured by the potentiostat. Hence, no reliable difference between the dark and illuminated currents could be measured in this case. Open circuit potential measurements of these Janus particles have shown a similarly positive potential value in the dark as PHI alone (-340 mV vs Ag/AgCl). Upon illumination however, a smaller negative shift can be observed (-40 mV vs -250 mV for PHI sheets without Pt), which is caused by the strong reduction activity of Pt, shifting the equilibrium value under illumination to more positive values than without the Pt cap (+340 mV vs +100mV vs Ag/AgCl, Figure **S16** vs Figure **3 c**). In the Pt-Janus particle case, the negative open circuit potential shift is followed by a positive transient behavior, akin to Figure **S8** for PHI alone in ambient water. It can hence be assumed that the PHI side of the Janus particle dominantly oxidizes H_2O_2, while electrons not only react on the PHI surface, but also on the Pt surface.

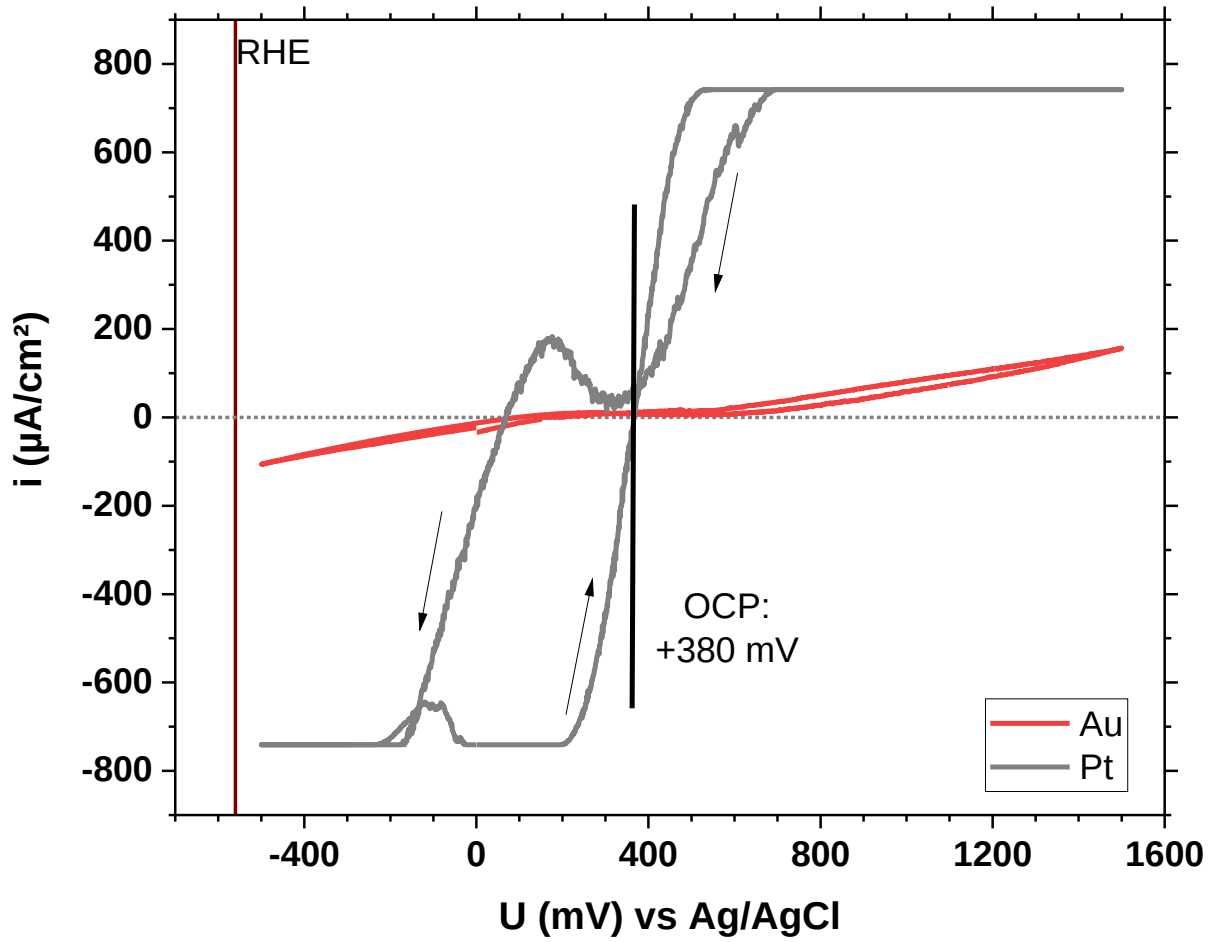

Figure S16: Cyclic voltammogram of a Pt wire and a gold plate in DI water containing 1 % H_2O_2. Pt (grey) catalyzes the reduction and oxidation of H_2O_2 more efficiently than Au (red). The depletion of reactants in the vecinity of Pt therefore causes a hysteresis and a catalytic wave. The open circuit potential is similar for both materials (+380 mV vs Ag/AgCl).

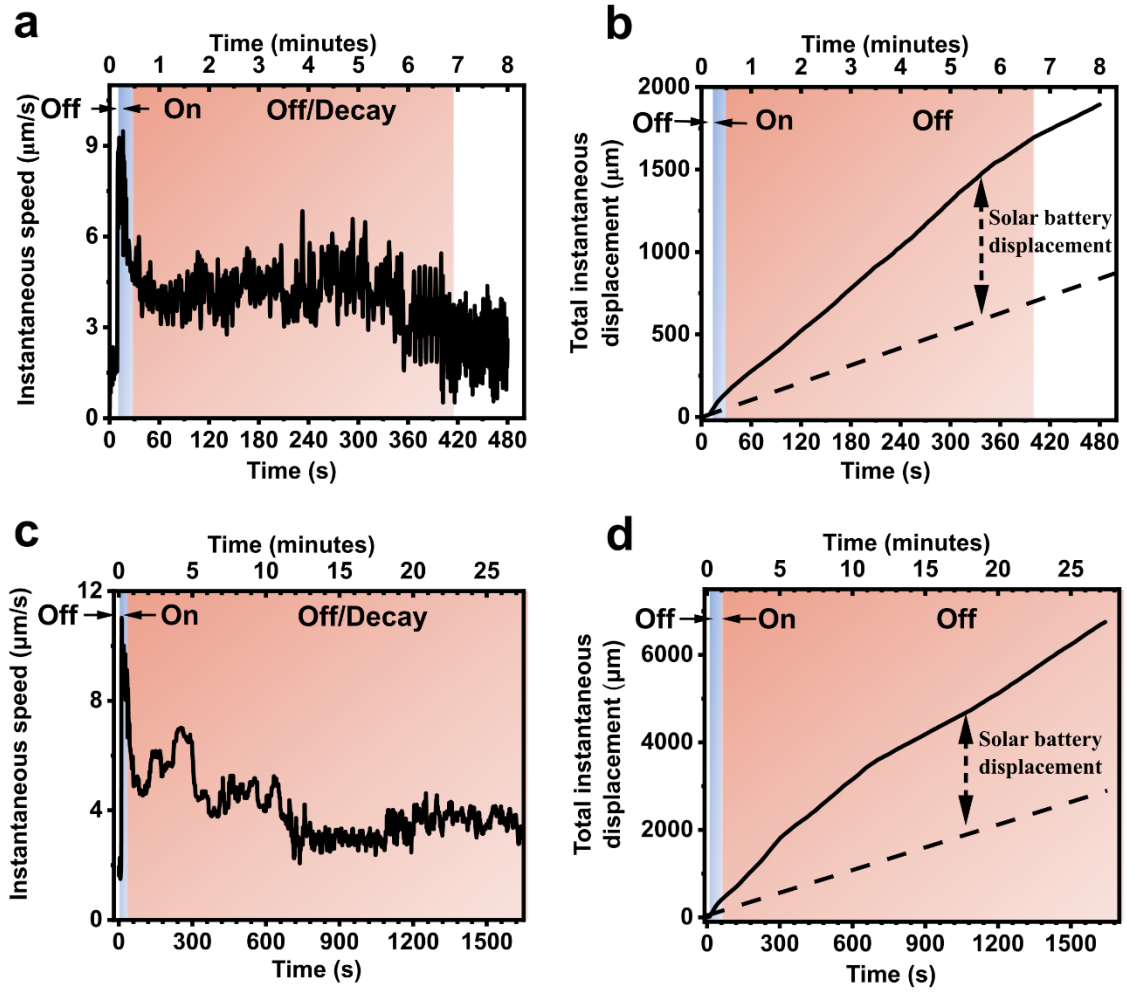

Figure S17. Solar battery swimming for longer prior illumination times. **a)** Solar battery swimming after 10 s of prior illumination, which leads to light-induced enhanced motion after UV illumination for 400 s (6.7 minutes, shown in orange-colored background). The active Brownian motion after the end of ballistic swimming (after 400 s) is shown with white background. The data represents an averaged instantaneous speed (N=5). **b)** Microswimmer total instantaneous displacement (distance traveled) over time extracted from **a)**. Dashed line here represents the total displacement in dark without illumination, estimated from the passive Brownian displacement before illumination. The solar battery displacement is 767 µm (2.2 times further than the passive Brownian displacement) in 400 s. **c**) Solar battery swimming after 30 s of illumination, which leads to light induced enhanced motion after UV illumination for 600-800 s (13 minutes). The swimming slows down after 800 s but the swimmers continue to swim ballistically up to 1800 s. The data represents an averaged instantaneous speed (N=10). **d)** Microswimmer total instantaneous displacement as shown in **c)**, reaching 3600 µm (2.16 times further than the passive Brownian displacement in the same duration) in 27 minutes. Some swimmers continue to swim even longer than half an hour, which is beyond the possible analysis time of our equipment (30 minutes), hence making the propulsion time and total instantaneous displacement difficult to estimate for longer initial illumination times than 30 s.

References

1. Nosaka Y & Nosaka AY (2017) Generation and Detection of Reactive Oxygen Species in Photocatalysis. *Chemical Reviews* 117(17):11302-11336.
2. Schneider JB, D.; Ye, J.; Puma, G. L.; Dionysiou, D. D., Eds. (2016) *Photocatalysis: Fundamentals and Perspectives* pp - 436.
3. Park H, Kim H-i, Moon G-h, & Choi W (2016) Photoinduced charge transfer processes in solar photocatalysis based on modified TiO2. *Energy & Environmental Science* 9(2):411-433.
4. Kang U, *et al.* (2015) Photosynthesis of formate from CO2 and water at 1% energy efficiency via copper iron oxide catalysis. *Energy & Environmental Science* 8(9):2638-2643.
5. Wardman P (1989) Reduction Potentials of One-Electron Couples Involving Free Radicals in Aqueous Solution. 18(4):1637-1755.
6. Evans DF & Upton MW (1985) Studies on singlet oxygen in aqueous solution. Part 1. Formation of singlet oxygen from hydrogen peroxide with two-electron oxidants. *Journal of the Chemical Society, Dalton Transactions* (6):1141-1145.
7. Dey S, *et al.* (2017) Molecular electrocatalysts for the oxygen reduction reaction. *Nature Reviews Chemistry* 1(12):0098.
8. Chen Z, Dinh H, & Miller E (2013) *Photoelectrochemical water splitting* (Springer publishing house New York) p 124.
9. Yi J, Bahrini C, Schoemaecker C, Fittschen C, & Choi W (2012) Photocatalytic Decomposition of H2O2 on Different TiO2 Surfaces Along with the Concurrent Generation of HO2 Radicals Monitored Using Cavity Ring Down Spectroscopy. *The Journal of Physical Chemistry C* 116(18):10090-10097.
10. Villa K, Manzanares Palenzuela CL, Sofer Z, Matějková S, & Pumera M (2018) Metal-Free Visible-Light Photoactivated C3N4 Bubble-Propelled Tubular Micromotors with Inherent Fluorescence and On/Off Capabilities. *ACS Nano* 12(12):12482-12491.
11. Ye Z, Sun Y, Zhang H, Song B, & Dong B (2017) A phototactic micromotor based on platinum nanoparticle decorated carbon nitride. *Nanoscale* 9(46):18516-18522.

Supplementary Movies

Supplementary Movie 1: **Magnetic control of PHI-Ni-Pt microswimmers** - Magnetic steering control demonstration of a PHI-Ni-Pt microswimmer in water containing 5% MeOH with video recorded for 15 s.

Supplementary Movie 2: **PHI-Pt microswimmers in 5% methanol** - Propulsion of PHI-Pt microswimmers in water containing 5% MeOH with video recorded for 15 s.

Supplementary Movie 3: **PHI-Au microswimmers in 5% methanol** - Propulsion of PHI-Au microswimmers in water containing 5% MeOH with video recorded for 15 s.

Supplementary Movie 4: **PHI-Pt microswimmers in 0.05% H_2O_2** - Propulsion of PHI-Pt microswimmers in water containing 0.05% H_2O_2 with video recorded for 15 s.

Supplementary Movie 5: **PHI-SiO_2 microswimmers in 0.5% H_2O_2** - Propulsion of PHI-SiO_2 microswimmers in water containing 0.5% H_2O_2 with video recorded for 15 s.

Supplementary Movie 6: **PHI-Pt microswimmer photo charging and solar battery swimming in 1% H_2O_2** - Off/on/off solar battery swimming of a PHI-Pt microswimmer in water containing 1% H_2O_2 with video recorded for 21 s.

Supplementary Movie 7: PHI-Pt microswimmers solar battery swimming for extend periods 1% H_2O_2 - Discharge swimming in PHI-Pt microswimmers in water containing 1% H_2O_2 with videos and left and right showing two different particles performing solar battery swimming under the same conditions with video recorded for 120 s.